Journal of Rock Mechanics and Geotechnical Engineering 14 (2022) 984–993

Contents lists available at ScienceDirect

Journal of Rock Mechanics and Geotechnical Engineering

journal homepage: www.jrmge.cn

Full Length Article

A modified Kozeny–Carman equation for predicting saturated hydraulic conductivity of compacted bentonite in confined condition

Kunlin Ruan [a], Xian-Lei Fu [b,*]

[a] Department of Civil and Environmental Engineering, Waseda University, Tokyo, 169-8555, Japan
[b] Jiangsu Key Laboratory of Urban Underground Engineering and Environmental Safety, Institute of Geotechnical Engineering, Southeast University, Nanjing, 210096, China

ARTICLE INFO

Article history:
Received 21 May 2021
Received in revised form
22 July 2021
Accepted 20 August 2021
Available online 12 November 2021

Keywords:
Kozeny–carman (KC) equation
Saturated hydraulic conductivity
Bentonite
Pore size distribution (PSD)
Specific surface area

ABSTRACT

Kozeny–Carman (KC) equation is a well-known relation between hydraulic conductivity and pore properties in porous material. The applications of KC equation to predicting saturated hydraulic conductivities of sands and non-expansive soils are well documented. However, KC equation is incapable of predicting saturated hydraulic conductivity of expansive soil (e.g. bentonite) well. Based on a new dual-pore system, this study modified KC equation for improving the prediction of saturated hydraulic conductivities of bentonites. In this study, an assumption that inter-layer space (micropore) has limited effect on fluid flow performance of compacted bentonite was adopted. The critical parameters including total porosity and total tortuosity in conventional KC equation were replaced by macroporosity and tortuosity of macropore, respectively. Macroporosity and microporosity were calculated by basal spacing of compacted bentonite, which was estimated by assuming that specific surface area is changeable during saturation process. A comprehensive comparison of bentonite's saturated hydraulic conductivity predictions, including modified KC equation proposed in this study, conventional KC equation, and prediction method based on diffuse double layer (DDL) theory, was carried out. It was found that the predicted saturated hydraulic conductivity of bentonites calculated using modified KC equation fitted the experimental data better than others to a certain extent.

1. Introduction

Deep geological disposal method was chosen by different countries for handling high-level nuclear waste from nuclear power industry (JNC, 1999; SKB, 2011). In a Japanese project, a multi-barrier system consisting of buffer material and natural rock is designed to prevent the leakage of nuclide waste. Bentonite and bentonite-based material are selected as buffer material due to their low hydraulic conductivity and superior swelling capability (Sun et al., 2009, 2013; Fu et al., 2021a,b, 2022).

Pore in compacted bentonite, which has been proved having crucial effect on mechanical properties, has received wide attention and been studied intensively. However, classification standard for pores in bentonite is not uniform. A generally accepted category (see Fig. 1) is: (1) inter-layer pore (micro-level), (2) inter-particle pore (pore in aggregates, meso-level), and (3) inter-aggregate pore (pore between aggregates, macro-level) (Pusch, 2001; Pusch and Yong, 2006; Romero, 2013; Chen et al., 2020). Some researchers (e.g. Sedighi and Thomas, 2014) combined meso-level and macro-level pores into new "macropore" (see Fig. 1). In general, mercury intrusion porosimetry (MIP) technology has been widely used to investigate pore size distribution (PSD) in compacted bentonites (Delage et al., 2006; Lloret et al., 2003). However, pores between two individual montmorillonite layers with diameter smaller than 3.7 nm (Xiong et al., 2016) cannot be determined using MIP. Therefore, X-ray diffraction (XRD), as a novel technology, is used to obtain pore characteristics in compacted bentonite for more precise results (Likos and Lu, 2006).

Hydraulic conductivity of compacted bentonite is strongly affected by PSD (Wang et al., 2013; Gao et al., 2021). Kozeny–Carman (KC) equation proposed by Kozeny (1927) and Carman (1937) associates hydraulic conductivity with porosity in porous material. In geotechnical engineering field, there is a consensus that KC equation only performs well with the hydraulic conductivity of

* Corresponding author.
E-mail address: fuxianlei@seu.edu.cn (X.-L. Fu).
Peer review under responsibility of Institute of Rock and Soil Mechanics, Chinese Academy of Sciences.

https://doi.org/10.1016/j.jrmge.2021.08.010

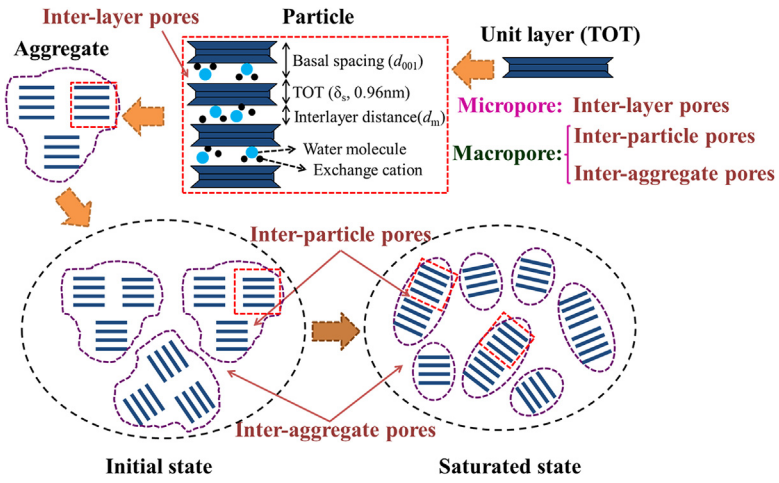

Fig. 1. Schematic diagram of fabric units of compacted bentonite and their developments under confined wetting.

sands but not clays. However, this view is just supported by partial demonstration. Chapuis and Aubertin (2003a,b) and Chapuis (2012) summarized experimental results of hydraulic conductivities of some clays, including kaolinite, illite, Boston blue clay, and Champlain clay (Olsen, 1960; Tavenas et al., 1983; Al-Tabbaa and Wood, 1987). It is apparently seen from Fig. 2a that KC equation can predict saturated hydraulic conductivities of non-expansive soils well. However, KC equation does not perform well for hydraulic conductivity of bentonite (Chen et al., 2020). For example, it can be seen from Fig. 2b that there are errors between predicted values calculated using KC equation and experimental data of different bentonites: MX-80 (Pusch, 2001), GMZ (Wen, 2006), Kunigel-V1 (Hasegawa, 2004), FEBEX (Villar, 2002), and Kunibon (Komine, 2008). Therefore, it is of paramount importance to improve KC equation for predicting saturated hydraulic conductivity of bentonite better.

In this study, attempts were made to modify KC equation for predicting saturated hydraulic conductivity of compacted bentonite more precisely. KC equation was modified based on a new dual-pore system in compacted bentonite. Basal spacing from changeable specific surface area during saturation was used for obtaining PSD. A comprehensive comparison of predicted saturated hydraulic conductivity for compacted bentonite was conducted according to modified KC equation proposed in this study, conventional KC equation, and prediction method based on diffuse double layer (DDL) theory reported in previous studies.

2. Modifying KC equation based on water flow mechanism

2.1. Microstructure of compacted bentonite and pore classification

Generally, microstructure of compacted bentonite consists of unit layer, particle, and aggregate (Jacinto et al., 2012). The microstructure of compacted bentonite is schematically shown in Fig. 1. Montmorillonite, the main composition of bentonite, is generally accepted as a 2:1 unit layer consisting of an alumina octahedral sheet sandwiched between two silica tetrahedral sheets (TOT, approximately 9.6 Å in thickness from Mitchell and Soga, 2005). Several unit layers are often combined in a face-to-face orientation and compose a particle subsequently. Furthermore, aggregates made up by several particles are formed.

MIP technology has been widely used to investigate PSD in the compacted bentonite. This method can retrieve the pore sizes at the range of 3.7 nm–500 μm (Delage et al., 2006; Xiong et al., 2016). However, the distance between unit layers is generally smaller than 3.7 nm in confined condition, which is important to the mechanical characteristics of bentonite. Therefore, XRD technology was adopted to evaluate pore system in compacted bentonite to make up for the deficiency of MIP technology (Holmboe et al., 2012). Basal spacing is transformed from the result of XRD into pore size by different microstructural hypothesizes. For example, Likos and Lu (2006) assumed quasicrystals uniformly distributed in bentonite. XRD can only measure inter-layer distance, but pore properties of aggregate and inter-aggregate are impossible to be obtained. Therefore, a novel pore classification was proposed by some scholars based on XRD (Likos and Lu, 2006; Sedighi and Thomas, 2014). They separated pores into micropores (i.e. inter-layer pores) and macropores (i.e. inter-particle pores and inter-aggregate pores) (see Fig. 1).

2.2. Modifying KC equation by water flow mechanism in different pores

Generally, pore properties have a great contribution to the flow characteristics of porous materials. Kozeny (1927) and Carman (1937) related the saturated hydraulic conductivity (k_{sat}) with saturated total porosity ($n_{total,s}$) as the KC equation. This equation was firstly proposed by Kozeny (1927) based on the assumption of a series of capillary tubes of equal length (Chapuis and Aubertin, 2003a,b). Carman (1937, 1938a,b, 1939) tried to apply this equation to calculating the hydraulic conductivity of saturated sands, soils, and clays by assuming that water moves around irregular shaped solid particles instead of straight channels. The KC equation is considered to be approximately valid for sand but inadequate for clays, which is because that the KC equation was established as per solid-fluid system (Lambe and Whitman, 1969; Domenico and Schwartz, 1997; Mitchell and Soga, 2005). However, this opinion lacks demonstration. Carman (1939) ascribed that the thin water layer attached at the surface of clayey particle could provide a solid-fluid interface for water flow. As shown in Fig. 2a, by comparing experimental results of hydraulic conductivities of kaolinite, illite, and Boston blue clay from Olsen (1960), Champlain clays from Tavenas et al. (1983), kaolinite from Al-Tabbaa and Wood (1987) with KC equation prediction database, Chapuis (2012) concluded that KC equation provided a good prediction for hydraulic conductivities of some clays. Applying this equation to bentonites, KC equation can be expressed as (Chen et al., 2020):

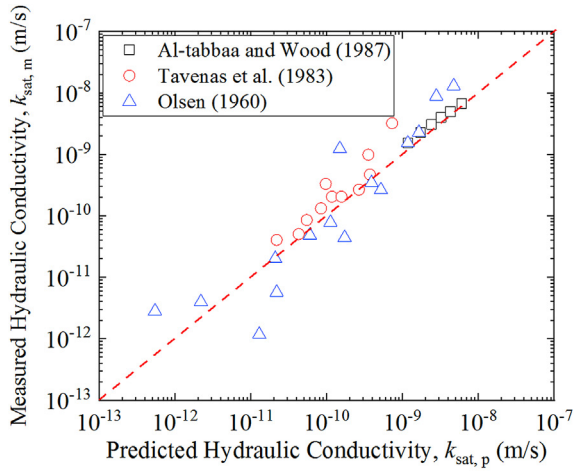

Fig. 2. Comparisons between testing results for different soils and prediction using KC equation: (a) non-expansive soils (Olsen, 1960; Tavenas et al., 1983; Al-Tabbaa and Wood, 1987) and (b) bentonites (Push, 2001; Villar, 2002; Hasegawa, 2004; Wen, 2006; Komine, 2008).

$$k_{sat} = \frac{\gamma_w}{\mu_w}\frac{C_s}{\tau_{total,s}^2 A_{bentonite,s}^2 \rho_d^2}\frac{n_{total,s}^3}{(1-n_{total,s})^2} \quad (1)$$

$$\tau_{total,s} = (1 - 0.5\ln n_{total,s})^{1/2} \quad (2)$$

$$\mu_w = g\nu_w \quad (3)$$

where ρ_d is the dry density of a specimen (g/cm^3), γ_w represents the unit weight of water (N/m^3, $\gamma_w = g\rho_w$), g is the gravitational constant (m/s^2), ν_w signifies the kinematic viscosity of water (m^2/s), C_s is a dimensionless shape constant recommended as 0.2 for soils (Chapuis and Aubertin, 2003b), $\tau_{total,s}$ is the saturated tortuosity of total pores, and $A_{bentonite}$ is the specific surface area of bentonite. However, for smectite-rich clays, the KC equation is not well applicable (see Fig. 2b). Therefore, it is necessary to modify the KC equation to predict hydraulic conductivity of expansive soils (e.g. compacted bentonite) better.

In this study, water categorized by their location in compacted bentonite is known to be: (1) water in inter-layer pore (inter-layer water), (2) water in inter-aggregate pore (inter-aggregate water), and (3) water in intra-aggregate pore (intra-aggregate water). The inter-layer water results from the hydration of exchangeable cations in montmorillonite layers (Cases et al., 1992). Since isomorphous substitutions of divalent cations for aluminum ion (Al^{3+}) in the octahedral sheet and Al^{3+} for silicon ion (Si^{4+}) in the tetrahedral sheet (Liu, 2013), the unit layer is always negative charged. After soil encounters water, the negative surface charge will attract water molecules orderly arranged on the surface of crystal layers (Olphen, 1977; Suzuki et al., 2005). The inter-layer water is viewed as immobile due to the attractive force between water molecule and unit layers (Bradbury and Baeyens, 2003; Pusch and Yong, 2006). Thus, inter-layer pore has a negligible contribution to the overall flow of water in compacted bentonite (Pusch and Yong, 2006; Chen et al., 2020). Water in inter-aggregate pores can be divided into free water and DDL water (Appelo and Wersin, 2007; Tachi et al., 2014). DDL water, which is partially constrained due to the interactions with charged surfaces, has much larger mobility than inter-layer water. Therefore, some researches viewed DDL water as mobile water (e.g. Chen et al., 2020). Intra-aggregate water is considered as moveable because the permeable tunnel between aggregates is considerable.

In this study, pore classification is followed as Likos and Lu (2006) and Sedighi and Thomas (2014) that micropore is defined as the inter-layer pore and macropore is defined as the pores excluding inter-layer pore. Combining the different water types mentioned above, the flow mechanism by pore size in this study can be concluded that macropore is the flow path for moveable water.

Most reports assumed unit layers as parallel coincidence sheets and moveable water flow path, as shown in Fig. 3a. Wang et al. (2021a) investigated the structure of montmorillonite via cryo-scanning electron microscopy (cryo-SEM) and atomic force microscope (AFM). They indicated that the montmorillonite could move laterally during saturation process (see Figs. 3b and 4). Similar phenomenon was reported by Tournassat et al. (2003) and Cadene et al. (2005). Montmorillonite surface overlapping occurs due to the horizontal movement of unit layers. Therefore, new flow path for moveable water in compacted bentonite was adopted in this study, as shown in Fig. 3b.

Following aforementioned discussion, this study replaced $n_{total,s}$ in conventional KC equation with $n_{macro,s}$ (saturated macroporosity), and $\tau_{total,s}$ was replaced by $\tau_{macro,s}$ (tortuosity of saturated macropore) as modified KC equation:

$$k_{sat} = \frac{\gamma_w}{\mu_w}\frac{C_s}{\tau_{macro,s}^2 A_{bentonite,s}^2 \rho_d^2}\frac{n_{macro,s}^3}{(1-n_{macro,s})^2} \quad (4)$$

$$\tau_{macro,s} = (1 - 0.5\ln n_{macro,s})^{1/2} \quad (5)$$

3. Micro and macropores with changeable specific surface area

3.1. Evaluation of specific surface areas and surface areas during saturation

Unit montmorillonite layers will interact with each other to form stacked layers, which are referred as crystal particle, due to the repulsion and attraction during hydration (see Fig. 4) (Liu, 2013; Chen et al., 2020). In the process of forming particles, individual unit layers will be arranged horizontally and parallel to each other, but they may not completely overlap in the vertical direction, as shown in Fig. 4 (Tournassat et al., 2011; Holmboe et al., 2012; Leao

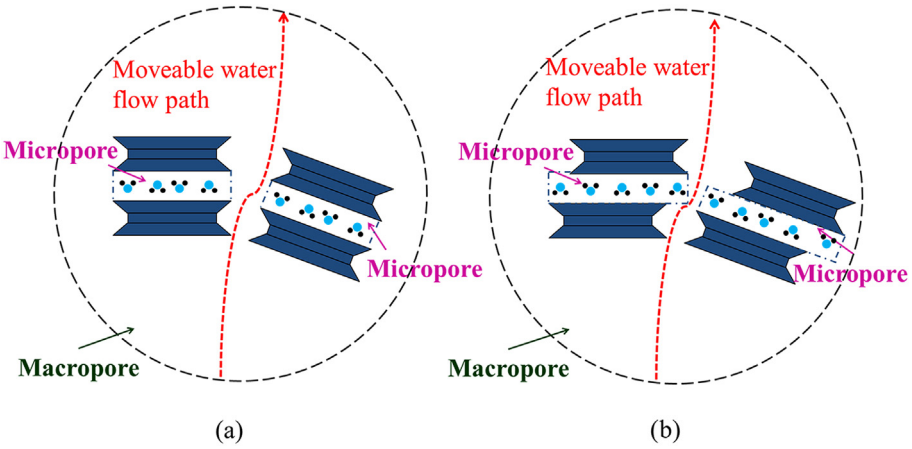

Fig. 3. Schematic diagram showing moveable water flow paths with different specific surface areas: (a) unchangeable specific surface area and (b) changeable specific surface area (adopted in this study).

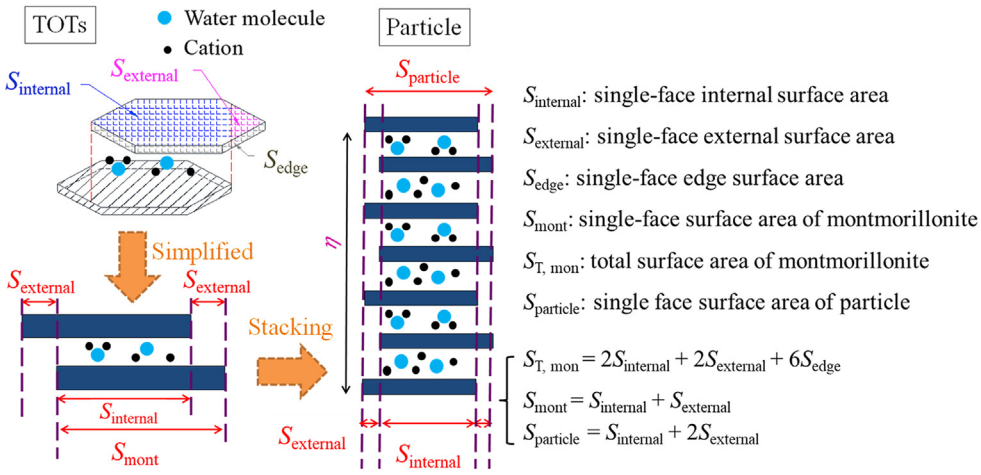

Fig. 4. Schematic diagram showing evaluation of surface area during saturation.

and Tuller, 2014; Tachi and Yotsuji, 2014; Lu and Zhang, 2020). This phenomenon was also observed by other technologies such as cryo-SEM and AFM (Dor et al., 2020; Wang et al., 2021a). As pointed by numerous studies (see Fig. 4), the specific surface areas of montmorillonite can be given as

$$A_{mont} = A_{external} + A_{internal} + A_{edge} \tag{6}$$

where A_{mont} is the specific surface area of montmorillonite, which can be obtained using ethylene glycol monoethyl ether technique (EGME); $A_{external}$ is the external specific surface area of montmorillonite, which can be obtained using gas sorption test; $A_{external}$ is the internal specific surface area of montmorillonite; and A_{edge} is the edge specific surface area of montmorillonite, which can be observed by AFM. A_{edge} is usually ignored because it is 1%–5% of A_{mont} (Tournassat et al., 2003; Cadene et al., 2005). Thus, Eq. (6) can be re-expressed as

$$A_{mont} = A_{external} + A_{internal} \tag{7}$$

As pointed by some studies (Tournassat et al., 2011; Chen et al., 2020), there are relations between specific areas and stacked unit layer number (η) as Eqs. (8) and (9). The number of stacked unit layers (η) would change with the degree of saturation (Saiyouri et al., 2004).

$$A_{internal} = \frac{2\eta - 2}{2\eta} A_{mont} = \frac{\eta - 1}{\eta} A_{mont} \tag{8}$$

$$A_{external} = \frac{2}{2\eta} A_{mont} = \frac{1}{\eta} A_{mont} \tag{9}$$

An S-shape relation was found between total suction (ψ) and stacked numbers (η) for sodium- and calcium-type bentonites (Na- and Ca-bentonite) by Chen et al. (2020) based on the experimental results from Saiyouri et al. (2004), and it could be fitted as

$$\eta = \frac{\eta_{max}}{1 + (\eta_{max}/\eta_{min} - 1)e^{z\psi}} \tag{10}$$

where η_{max} and η_{min} are the stacked numbers of dried and saturated specimens, respectively; and z is the fitting parameter. As reported by Chen et al. (2020), for Na-bentonite, $\eta_{max} = 350$, $\eta_{min} = 10$, and $z = -0.17$; for Ca-bentonite, $\eta_{max} = 100$, $\eta_{min} = 10$, and $z = -0.14$. Moreover, specific surface area of bentonite can be calculated following Komine and Ogata (1996, 2004):

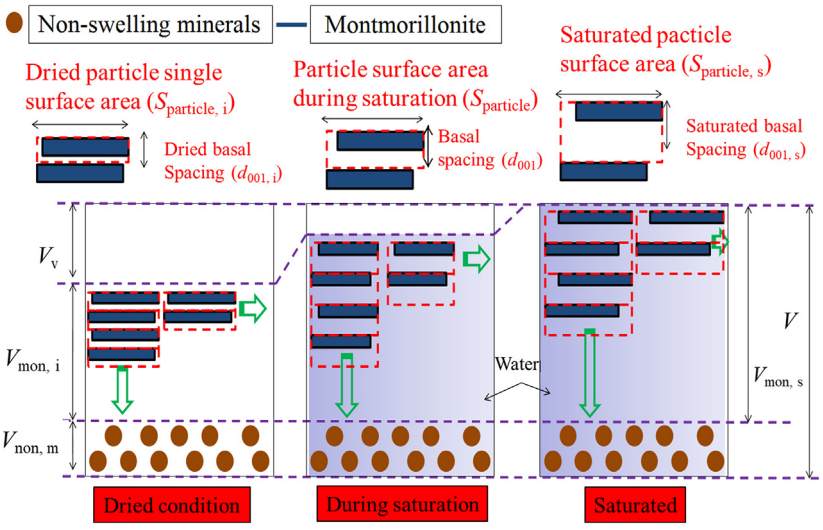

Fig. 5. Schematic diagram of basal spacing evaluation during saturation.

$$A_{bentonite} = A_{mont}C_m + A_{non,m}(1 - C_m) \tag{11}$$

where $A_{non,m}$ is the specific surface area of non-montmorillonite (0 m^2/g was adopted from Komine and Ogata (2004)), and C_m is the montmorillonite content in bentonite. Meanwhile, it can be seen from Fig. 4 that the relations between single-face surface areas can be given as Eq. (12) by assuming the unit montmorillonite layer as an octahedron.

$$S_{T,mon} = 2S_{external} + 2S_{internal} + 6S_{edge} \tag{12}$$

$$S_{mont} = S_{external} + S_{internal} \tag{13}$$

$$S_{particle} = 2S_{external} + S_{internal} \tag{14}$$

where $S_{internal}$, $S_{external}$, and S_{edge} are the single-face internal, external, and edge surface areas of montmorillonite unit layer (m^2), respectively; S_{mont} and $S_{T,mon}$ are the single-face and total surface areas of montmorillonite unit layer (m^2), respectively; and $S_{particle}$ is the single-face surface area of particle (m^2). Single-face edge surface area is ignored in this study following the discussion about the edge specific surface area as mentioned above. Thus, Eq. (12) can be re-given as

$$S_{T,mon} = 2S_{external} + 2S_{internal} = 2S_{mont} \tag{15}$$

Additionally, as per the relations between $A_{external}$, $A_{internal}$, and A_{mont} in Eqs. (8) and (9), the relations between single-face surface areas and stacked number can be expressed as

$$S_{internal} = \frac{\eta - 1}{\eta} S_{mont} \tag{16}$$

$$S_{external} = \frac{1}{\eta} S_{mont} \tag{17}$$

3.2. Determination of basal spacing in saturated state based on changeable specific surface area

For calculating the saturated basal spacing, it was assumed that the change of pore volume during saturation in confined condition is dominated by the volume change between unit layers (see Fig. 5). Thus, a relationship between saturated montmorillonite volume ($V_{mon,s}$) and initial montmorillonite volume in dried condition ($V_{mon,i}$) can be expressed as

$$\frac{V_{mon,s}}{V_{mon,i}} = \frac{mS_{particle,s}d_{001,s}}{mS_{particle,i}d_{001,i}} = \frac{S_{particle,s}d_{001,s}}{S_{particle,i}d_{001,i}} \tag{18}$$

where $S_{particle,s}$ is the saturated single-face surface area of particle, $S_{particle,i}$ is the initial single-face surface area of particle in dried condition, $d_{001,s}$ is the saturated basal spacing, $d_{001,i}$ is the initial basal spacing in dried condition (9.8 Å for this study), and m is the total number of unit layer in bentonite. The relationship between $V_{mon,s}$ and initial $V_{mon,i}$ can also be formed as

$$\frac{V_{mon,s}}{V_{mon,i}} = \frac{V - V_{non,m}}{V_{mon,i}} = \frac{m_s/\rho_d - m_s(1 - C_m)/\rho_{non,m}}{m_s C_m/\rho_{mon}} = \frac{1/\rho_d - (1 - C_m)/\rho_{non,m}}{C_m/\rho_{mon}} \tag{19}$$

where $V_{non,m}$ and V are the non-montmorillonite and total volumes in compacted bentonite, respectively; m_s is the total dry mass of bentonite; and ρ_{mon} and $\rho_{non,m}$ are the dry densities of montmorillonite and non-montmorillonite, respectively ($\rho_{mon} = \rho_{non,m} = 2.8$ g/cm^3 for this study, from Holmboe et al. (2012)). Combining Eqs. (18) and (19), a new relation can be obtained as

$$\frac{S_{particle,s}d_{001,s}}{S_{particle,i}d_{001,i}} = \frac{1/\rho_d - (1 - C_m)/\rho_{non,m}}{C_m/\rho_{mon}} \tag{20}$$

Therefore, saturated basal spacing ($d_{001,s}$) can be easily formed:

$$d_{001,s} = \frac{[1/\rho_d - (1 - C_m)/\rho_{non,m}]S_{particle,i}d_{001,i}}{A_{particle,s}C_m/\rho_{mon}} \tag{21}$$

Fig. 6 shows calculated saturated basal spacings of MX-80, GMZ, Kunigel-V1, Kunibon, and FEBEX bentonites as per Eq. (21). Detailed physical properties of these five bentonites in the literature are summarized in Table 1. MX-80, GMZ, and Kunigel-V1 are Na-bentonites; Kunibon is Ca-bentonite; and FEBEX is considered as

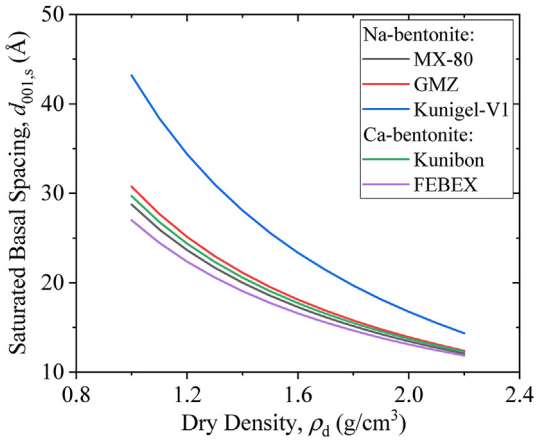

Fig. 6. Predicted basal spacings of bentonites in saturated state in this study.

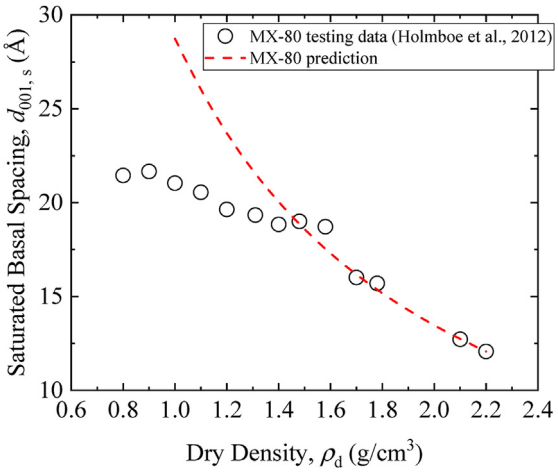

Fig. 7. Predicted basal spacings of MX-80 in saturated state in this study versus experimental results (Holmboe et al., 2012).

Ca–Mg-bentonite (Villar, 2002; Villar et al., 2012). However, FEBEX was viewed as Ca-bentonite in this study because its Ca exchangeable capacity was higher than that of Mg (see Table 1). As shown in Fig. 6, saturated basal spacing decreased with increasing dry density of bentonite. This phenomenon was consistent with the results obtained by Villar et al. (2012) and Pusch and Yong (2006). The comparison between saturated MX-80 basal spacings calculated using Eq. (21) and experimental results obtained by Holmboe et al. (2012) is indicated in Fig. 7. It can be seen that Eq. (21) fits well with experimental results in high dry density (>1.5 g/cm^3). For low dry density, the prediction is somewhat higher, which may be attributed to osmotic swelling between particles that leads to the pore volume change in compacted specimen.

3.3. Calculation for microporosity and macroporosity

Montmorillonite microporosity ($n_{monmicro}$) can be expressed as

$$n_{monmicro} = \frac{V_{il}}{V_{mon}} \tag{22}$$

where V_{il} and V_{mon} are the inter-layer and montmorillonite volumes, respectively.

Saturated montmorillonite microporosity ($n_{monmicro,s}$) can be expressed as

$$n_{monmicro,s} = \frac{V_{il,s}}{V_{mon,s}} \tag{23}$$

where $V_{il,s}$ and $V_{mon,s}$ are the saturated inter-layer and montmorillonite volumes, respectively.

As shown in Fig. 8, saturated inter-layer volume can be given as

$$V_{il,s} = mS_{particle,s}(d_{001,s} - \delta_s) \tag{24}$$

where δ_s is the thickness of unit layer (9.6 Å for this study from Komine and Ogata (2004)). Saturated montmorillonite volume can be presented by

$$V_{mon,s} = mS_{particle,s}d_{001,s} \tag{25}$$

Combining Eqs. 22–25, saturated montmorillonite microporosity ($n_{monmicro,s}$) can be formed:

$$n_{monmicro,s} = \frac{mS_{particle,s}(d_{001,s} - \delta_s)}{mS_{particle,s}d_{001,s}} = \frac{d_{001,s} - \delta_s}{d_{001,s}} \tag{26}$$

The equation for calculating saturated bentonite microporosity can be inspired by Eq. (11) as

$$n_{micro,s} = n_{monmicro,s}C_m + n_{nonmicro,s}(1 - C_m) \tag{27}$$

where $n_{nonmicro,s}$ is the saturated non-montmorillonite microporosity ($n_{nonmicro,s} = 0$ for this study). Saturated bentonite macroporosity ($n_{macro,s}$) can be calculated from total saturated porosity ($n_{total,s}$):

$$n_{total,s} = 1 - \frac{\rho_d}{G_s} \tag{28}$$

$$n_{macro,s} = n_{total,s} - n_{micro,s} \tag{29}$$

where G_s is the specific gravity.

Saturated bentonite microporosity and macropososity changing with dry density are presented in Fig. 9. It can be seen that the saturated microporosity and macropososity decrease with increasing dry density.

Table 1
Physical properties of bentonites.

Physical property	MX-80[a]	GMZ[b]	Kunigel-V1[c]	Kunibon[c]	FEBEX[a]
Bentonite type	Na	Na	Na	Ca	Ca
Montmorillonite specific surface area (m^2/g)[c]	810				
Non-montmorillonite specific surface area (m^2/g)[c]	0				
Specific density (g/cm^3)	2.82	2.66	2.79	2.71	2.7
Liquid limit (%)	526	275			102
Plastic limit (%)	46	38			53
Montmorillonite content (%)	83	75.4	48	80	92
CEC (meq/100 g)	65	77.3	73.2	79.6	102 ± 4
EXC_{Na} (meq/100 g)	46	43.36	40.5	11.9	27 ± 1
EXC_{Ca} (meq/100 g)	23	14.57	28.7	58.5	35 ± 2
EXC_{Mg} (meq/100 g)	6	6.17	3	8.35	31 ± 3
EXC_{K} (meq/100 g)		2.51	0.9	1.33	

Note: [a] from Villar et al. (2012); [b] from Ye et al. (2014); [c] from Komine and Ogata (2004).

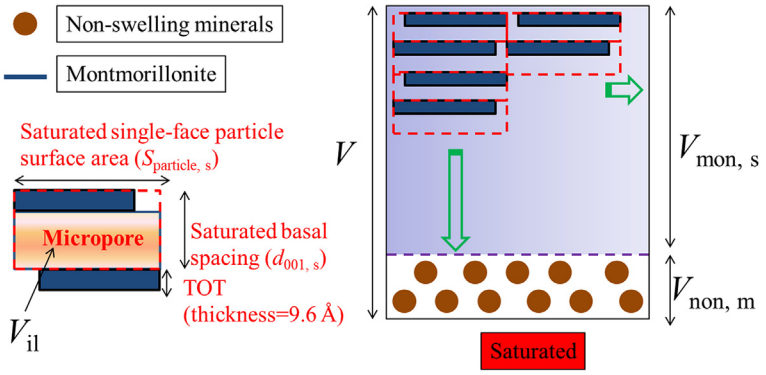

Fig. 8. Schematic diagram showing the calculation of microporosity in saturated state.

4. Verification of modified KC equation

Fig. 10 indicates saturated hydraulic conductivity of MX-80 (Pusch, 2001; Karnland et al., 2008; Komine, 2021), GMZ (Wen, 2006; Zhu et al., 2013; Wang et al., 2021b), Kunigel-V1 (Hasegawa, 2004; Komine, 2008; Satamatsu, 2021), FEBEX (Villar, 2002), and Kunibon (Komine, 2008) bentonites. Among the results in the literature, the hydraulic conductivities of most bentonites were measured based on falling head method with different apparatus, expect for Komine (2008, 2021) who obtained hydraulic conductivities as per Terzaghi one-dimensional consolidation theory. Predicted saturated hydraulic conductivity calculated using conventional KC equation and modified KC equation are presented in Fig. 10. As shown in Fig. 10, predicted values using modified KC equation fit much better with experimental results compared with those of conventional KC equation, especially for MX-80, GMZ, and FEBEX bentonites.

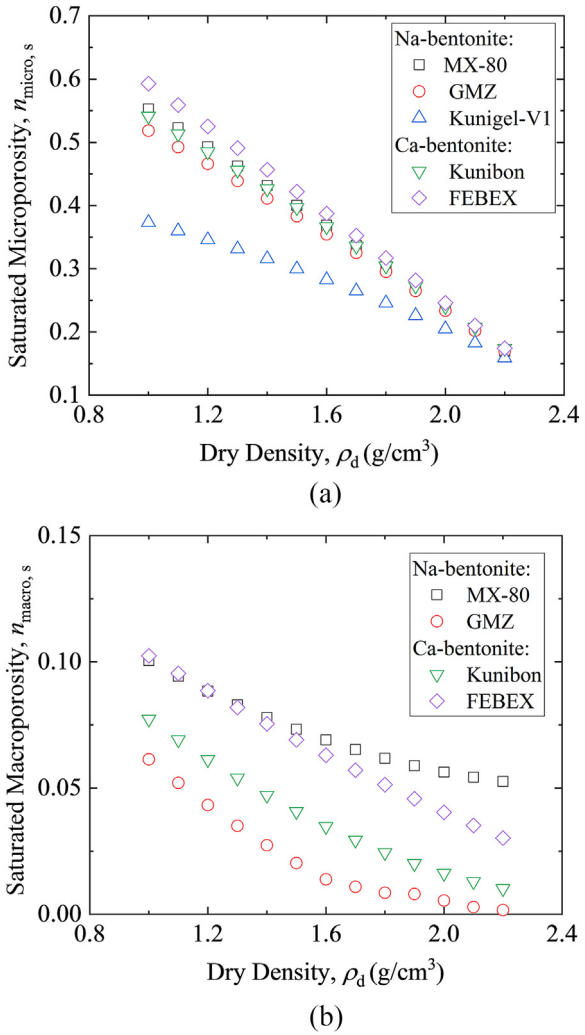

Fig. 9. Saturated (a) microporosity and (b) macropososity for different bentonites.

Based on modified DDL theory, Komine (2008) proposed a prediction method for saturated hydraulic conductivity of bentonite, which inferred water paths through the distance between two parallel plants by assuming that flow velocity of water between montmorillonite controls the flow velocity of water in bentonite. Meanwhile, it was supposed that water flow is two-dimensional and water is incompressible. The equation by Komine (2008) can be given as

$$k_{sat} = \frac{1}{CEC}\sum_i [EXC_i k_{sat,i}] \tag{30}$$

where $k_{sat,i}$ is the hydraulic conductivity of exchangeable cation i, EXC_i is the exchange capacity of the exchangeable cation i, and CEC is the cation exchange capacity of bentonite.

Fig. 11 reveals the predicted saturated hydraulic conductivity using the modified KC equation and prediction method based on DDL theory from Komine (2008). As we can see from Fig. 11a, for MX-80 bentonite, DDL theory performs better for the results from Komine (2021). Modified KC equation in this study fits better with the results from Pusch (2001) and Karnland et al. (2008). For GMZ bentonite, it can be easily concluded from Fig. 11b that modified KC prediction is closer to all testing data than DDL theory. For FEBEX bentonite in Fig. 11c, in the case of low dry density, modified KC equation performs better than DDL theory. For the high dry density (>1.5 g/cm^3), both two methods predict the hydraulic conductivity well.

5. Conclusions

Conventional KC equation cannot predict saturated hydraulic conductivity of bentonite well. A double pore system (i.e. micro and macropores) was raised after discussing water flow mechanisms in bentonite. It was assumed that macropore is the flow path for moveable water. Macroporosity and tortuosity of macropore were introduced into conventional KC equation to propose a modified KC equation. Basal spacing was estimated by assuming that the change of pore volume during saturation in confined condition is only controlled by the volume change between unit layers.

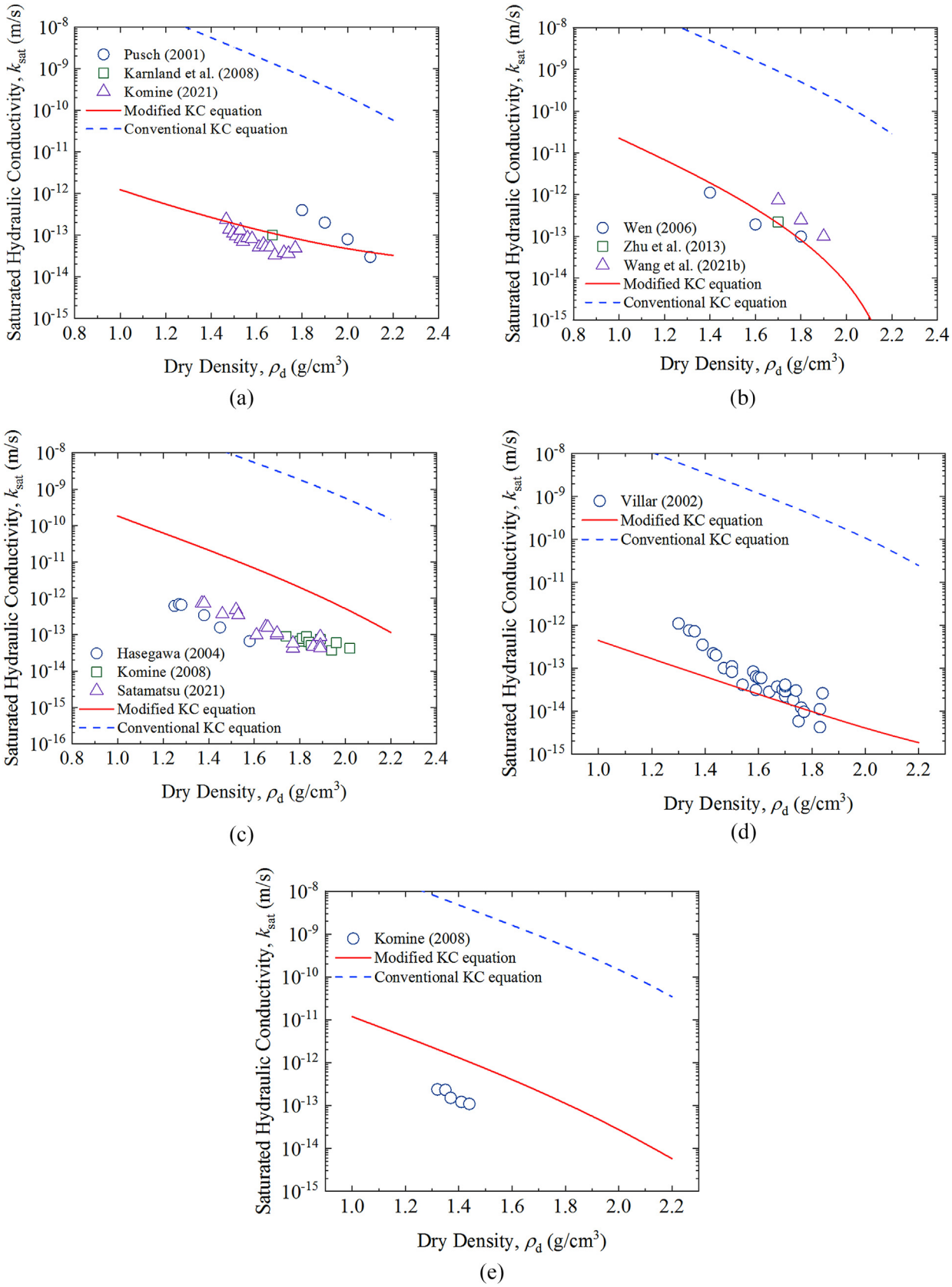

Fig. 10. Predicted saturated hydraulic conductivities of (a) MX-80, (b) GMZ, (c) Kunigel-V1, (d) FEBEX, and (e) Kunibon using conventional KC and modified KC equations changing with dry density from the literature (Push, 2001; Villar, 2002; Hasegawa, 2004; Wen, 2006; Karnland et al., 2008; Komine, 2008, 2021; Zhu et al., 2013; Wang et al., 2021b; Satamatsu, 2021).

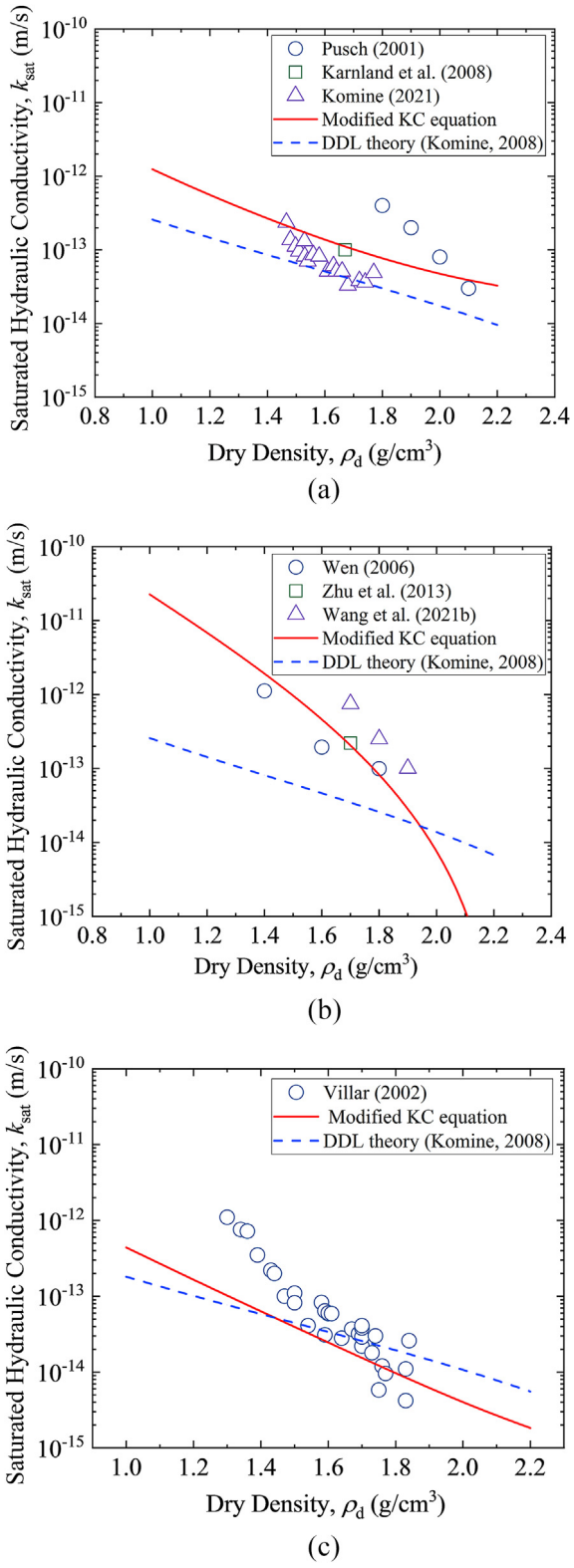

Fig. 11. Predicted saturated hydraulic conductivities by the modified KC equation and DDL theory for (a) MX-80, (b) GMZ, and (c) FEBEX (Push, 2001; Villar, 2002; Wen, 2006; Karnland et al., 2008; Komine, 2008, 2021; Zhu et al., 2013; Wang et al., 2021b).

Macroporosity and microporosity were obtained from basal spacing and changeable specific surface.

Saturated hydraulic conductivities of five bentonites (Na-type: MX-80, GMZ and Kunigel-V1; Ca-type: Kunibon and FEBEX) reported in previous studies were used to verify the accuracy of modified KC equation. Results showed that the predicted saturated hydraulic conductivities of bentonites calculated using modified KC equation fitted the experimental data better than those calculated using conventional KC equation and prediction method based on DDL theory to a certain extent.

Declaration of competing interest

The authors declare that they have no known competing financial interests or personal relationships that could have appeared to influence the work reported in this paper.

Acknowledgments

We acknowledge the support from the Ministry of Economy, Trade, and Industry (METI) of Japan and funding support from Postgraduate Research & Practice Innovation Program of Jiangsu Province, China (Grant No. KYCX21_0122).

List of symbols

$A_{non,m}$	Specific surface area of non-montmorillonite
A_{mont}	Specific surface area of montmorillonite
$A_{external}$	External specific surface area of montmorillonite
$A_{internal}$	Internal specific surface area of montmorillonite
A_{edge}	Edge specific surface area of montmorillonite
$S_{internal}$	Single-face internal surface area of montmorillonite unit layer
$S_{external}$	Single-face external surface area of montmorillonite unit layer
S_{edge}	Single-face edge surface area of montmorillonite unit layer
S_{mont}	Single-face surface area of montmorillonite unit layer
$S_{T,mon}$	Total surface area of montmorillonite unit layer
$S_{particle}$	Single-face surface area of particle
$d_{001,s}$	Basal spacing of saturated specimen
$d_{001,i}$	Basal spacing of dried specimen
C_m	Montmorillonite content in bentonite
k_{sat}	Saturated hydraulic conductivity
$k_{sat,m}$	Measured saturated hydraulic conductivity
$k_{sat,p}$	Predicted saturated hydraulic conductivity
m	Total number of unit layer in bentonite
$n_{total,s}$	Bentonite saturated total porosity
$n_{macro,s}$	Saturated bentonite macroporosity
$n_{micro,s}$	Saturated bentonite microporosity
$n_{nonmicro,s}$	Saturated non-montmorillonite microporosity
$n_{monmicro}$	Montmorillonite microporosity
$n_{monmicro,s}$	Saturated montmorillonite microporosity
V	Total volume of bentonite
V_m	Montmorillonite volume
$V_{non,m}$	Non-montmorillonite volume
$V_{mon,i}$	Montmorillonite volume in dry condition
$V_{mon,s}$	Saturated montmorillonite volume
V_{il}	Inter-layer volume
$V_{il,s}$	Saturated inter-layer volume
ρ_d	Dry densities of bentonite
ρ_{mon}	Dry densities of montmorillonite
$\rho_{non,m}$	Dry densities of non-montmorillonite
δ_s	Thickness of unit layer
η	Number of stacked unit layers
$\tau_{total,s}$	Tortuosity of saturated total pores
$\tau_{macro,s}$	Tortuosity of saturated macropore
ν_w	Kinematic viscosity of water

References

Al-Tabbaa, A., Wood, D.M., 1987. Some measurements of the permeability of kaolin. Geotechnique 37 (4), 499–503.

Appelo, C.A.J., Wersin, P., 2007. Multicomponent diffusion modeling in clay systems with application to the diffusion of tritium, iodide, and sodium in Opalinus clay. Environ. Sci. Technol. 41, 5002–5007.

Bradbury, M.H., Baeyens, B., 2003. Porewater chemistry in compacted re-saturated MX-80 bentonite. J. Contam. Hydrol. 61 (1–4), 329–338.

Cadene, A., Durand-Vidal, S., Turq, P., Brendle, J., 2005. Study of individual Na-montmorillonite particles size, morphology, and apparent charge. J. Colloid Interface Sci. 285 (2), 719–730.

Carman, P.C., 1937. Fluid flow through granular beds. Trans. Inst. Chem. Eng. 15, 150–166.

Carman, P.C., 1938a. Fundamental principles of industrial filtration (A critical review of present knowledge). Trans. Inst. Chem. Eng. 16, 168–188.

Carman, P.C., 1938b. Determination of the specific surface of powders I. J. Chem. Soc. Trans. 57, 225–234.

Carman, P.C., 1939. Permeability of saturated sands, soils and clays. J. Agric. Sci. 29, 263–273.

Cases, J.M., Berend, I., Besson, G., Francois, M., Uriot, J.P., Thomas, F., Poirier, J.E., 1992. Mechanism of adsorption and desorption of water-vapor by homoionic montmorillonite. 1. The sodium-exchanged form. Langmuir 8 (11), 2730–2739.

Chapuis, R.P., Aubertin, M., 2003a. Predicting the Coefficient of Permeability of Soils Using the Kozeny–Carman Equation. É cole Polytechnique de Montréal. Technical Report EPM-RT-2003–03, Département Des Gnies Civil. Géologique et des Mines.

Chapuis, R.P., Aubertin, M., 2003b. On the use of the Kozeny–Carman equation to predict the hydraulic conductivity of soils. Can. Geotech. J. 40 (3), 616–628.

Chapuis, R.P., 2012. Predicting the saturated hydraulic conductivity of soils-a review. Bull. Eng. Geol. Environ. 71, 401–434.

Chen, T., Sedighi, M., Jivkov, A.P., Seetharam, S.C., 2020. A model for hydraulic conductivity of compacted bentonite - inclusion of microstructure effects under confined wetting. Geotechnique. https://doi.org/10.1680/jgeot.19.P.088.

Delage, P., Marcial, D., Cui, Y.J., Ruiz, X., 2006. Ageing effects in a compacted bentonite: a microstructure approach. Geotechnique 56 (5), 291–304.

Domenico, P.A., Schwartz, F.W., 1997. Physical and Chemical Hydrogeology, second ed. John Wiley & Sons, NY, USA.

Dor, M., Levi-Kalisman, Y., Day-Stirrat, R.J., Mishael, Y., Emmanuel, S., 2020. Assembly of clay mineral platelets, tactoids, and aggregate: effect of mineral structure and solution salinity. J. Colloid Interface Sci. 566, 163–170.

Fu, X.L., Zhang, R., Reddy, K.R., Li, Y.C., Yang, Y.L., Du, Y.J., 2021a. Membrane behavior and diffusion properties of sand/SHMP-amended bentonite vertical cutoff wall backfill exposed to lead contamination. Eng. Geol. 284, 106037.

Fu, X.L., Wu, H.L., Zhang, R., Jiang, Z.Y., Reddy, K.R., Du, Y.J., 2021b. Heavy metals containment by vertical cutoff walls backfilled with novel reactive magnesium-activated slag-bentonite-sand: membrane and diffusion behavior. J. Clean. Prod. 328, 129623.

Fu, X.L., Shen, S.Q., Reddy, K.R., Yang, Y.L., Du, Y.J., 2022. Hydraulic conductivity of sand/biopolymer-amended bentonite backfills in vertical cutoff walls permeated with lead solutions. J. Geotech. Geoenviron. Eng. 148 (2), 04021186.

Gao, Y., Li, Z., Sun, D.A., Yu, H.H., 2021. A simple method for predicting the hydraulic properties of unsaturated soils with different void ratios. Soil Tillage Res. 209, 104913.

Hasegawa, T., 2004. Investigation on the Effect of Seawater to Hydraulic Property and Wetting Process of Bentonite. Central Research Institute of Electric Power Industry, Japan. Technical Report No. N04005.

Holmboe, M., Wold, S., Jonsson, M., 2012. Porosity investigation of xompacted bentonite using XRD profile modeling. J. Contam. Hydrol. 128, 19–32.

Jacinto, A., Villar, M., Ledesma, A., 2012. Influence of water density on the water-retention curve of expansive clays. Geotechnique 62 (8), 657–667.

JNC, 1999. Technical Reliability of the Geological Disposal for High Level Radioactive Waste in Japan Geological Disposal Research and Development. . Second compiled General report. Japan Nuclear Cycle Development Institute. JNC TN1400 99–120.

Karnland, O., Nilsson, U., Weber, H., Wersin, P., 2008. Sealing ability of Wyoming bentonite pellets foreseen as buffer material-laboratory results. Phys. Chem. Earth 33, S472–S475.

Komine, H., Ogata, N., 1996. Prediction for swelling characteristics of compacted bentonite. Can. Geotech. J. 33, 11–22.

Komine, H., Ogata, N., 2004. Prediction swelling characteristics of bentonites. J. Geotech. Geoenviron. Eng. 130 (8), 818–829.

Komine, H., 2008. Theoretical equations on hydraulic conductivities of bentonite-based buffer and backfill for underground disposal of radioactive wastes. J. Geotech. Geoenviron. Eng. 134 (4), 497–508.

Komine, H., 2021. Cation filtration of montmorillonite on hydraulic conductivities of some bentonites in artifical seawater. J. Geotech. Geoenviron. Eng. 147 (5), 06021002.

Kozeny, J., Sci, R. Acad, Vienna, 1927. Ueber kapillare leitung der wasser in boden. Proc. Class I 136, 271–306.

Lambe, T.W., Whitman, R.V., 1969. Soil Mechanics, first ed. John Wiley & Sons, NY, USA.

Leao, T.P., Tuller, M., 2014. Relating soil specific surface area, water film thickness, and water vapor adsorption. Water Resour. Res. 50 (10), 7873–7885.

Likos, W.J., Lu, N., 2006. Pore-scale analysis of bulk volume change from crystalline interlayer swelling in Na^{+}- and Ca^{2+}-smectite. Clay Clay Miner. 54 (4), 515–528.

Liu, L.C., 2013. Prediction of swelling pressures of different types of bentonite in dilute solutions. Colloid. Surface. Physicochem. Eng. Aspect. 434, 303–318.

Lu, N., Zhang, C., 2020. Separating external and internal surface areas of soil particles. J. Geotech. Geoenviron. Eng. 146 (2), 04019126.

Lloret, A., Villar, M.V., Sanchez, M., Gen, A., Pintado, X., Alonso, E.E., 2003. Mechanical behaviour of heavily compacted bentonite under high suction changes. Geotechnique 53 (1), 27–40.

Mitchell, J.K., Soga, K., 2005. Fundamentals of Soil Behavior, third ed. John Wiley & Sons, NY, USA.

Olphen, H.V., 1977. An Introduction to Clay Colloid Chemistry, second ed. John Wiley & Sons, NY, USA.

Olsen, H.W., 1960. Hydraulic flow through saturated clays. Clay Clay Miner. 9 (1), 131–161.

Pusch, R., 2001. The Microstructure of MX-80 Clay with Respect to its Bulk Physical Properties under Different Environmental Conditions. Swedish Nuclear Fuel and Waste Management Co., Stockholm, Sweden. Technical Report No. SKB-TR-01-08.

Pusch, R., Yong, R.N., 2006. Microstructure of Smectite Clays and Engineering Performance, first ed. Taylor and Francis, NY, USA.

Romero, E., 2013. A microstructural insight into compacted clayey soils and their hydraulic properties. Eng. Geol. 165, 3–19.

Satamatsu, A., 2021. Measurement of Hydraulic Conductivity of Compacted Bentonite by the Falling Head Test Method. MSc Thesis. Waseda University, Tokyo, Japan.

Sedighi, M., Thomas, H.R., 2014. Microporosity evolution in compacted swelling clays—a chemical approach. Appl. Clay Sci. 101, 608–618.

Saiyouri, N., Tessier, D., Hicher, P.Y., 2004. Experimental study of swelling in unsaturated compacted clays. Clay Miner. 39 (4), 469–479.

SKB, 2011. Long-term Safety for the Final Repository for Spent Nuclear Fuel at Forsmark-Main Report of the SR-Site Project, vol. 1. Swedish Nuclear Fuel and Waste Management Co., Stockholm, Sweden. Technical Report No. TR-11-01.

Sun, D.A., Cui, H.B., Sun, W.J., 2009. Swelling of compacted sand-bentonite mixtures. Appl. Clay Sci. 43 (3), 485–492.

Sun, D.A., Zhang, J.Y., Zhang, J.R., Zhang, L., 2013. Swelling characteristics of GMZ bentonite and its mixtures with sand. Appl. Clay Sci. 83, 224–230.

Suzuki, S., Prayongphan, S., Ichikawa, Y., Chae, B., 2005. In suit observations of the swelling of bentonite aggregates in NaCl solution. Appl. Clay Sci. 29 (2), 89–98.

Tachi, Y., Yotsuji, K., 2014. Diffusion and sorption of Cs^{+}, Na^{+}, I and HTO in compacted sodium montmorillonite as a function of porewater salinity: integrated sorption and diffusion model. Geochem. Cosmochim. Acta 132, 75–93.

Tachi, Y., Yotsuji, K., Suyama, T., Ochs, M., 2014. Integrated sorption and diffusion model for bentonite, Part 2: porewater chemistry, sorption and diffusion modeling in compacted system. J. Nucl. Sci. Technol. 51 (10), 1191–1204.

Tavenas, F., Jean, P., Leblond, P., Leroueil, S., 1983. The permeability of natural soft clays. Part II: permeability characteristics. Can. Geotech. J. 20, 645–660.

Tournassat, C., Neaman, A., Villiéras, F., Bosbach, D., Charlet, L., 2003. Nanomorphology of montmorillonite particles: estimation of the clay edge sorption site density by low-pressure gas adsorption and AFM observations. Am. Mineral. 88 (11–12), 1989–1995.

Tournassat, C., Bizi, M., Braibant, G., Crouzet, C., 2011. Influence of montmorillonite tactoid size on Na-Ca cation exchange reactions. J. Colloid Interface Sci. 364 (2), 443–454.

Villar, M.V., 2002. Thermo-hydro-mechanical characterisation of a bentonite from Cabo de Gata. PhD Thesis. Universidad Complutense de Madrid, Madrid, Spain.

Villar, M.V., Espina, R.G., Nebot, L.G., 2012. Basal spacings of smectite in compacted bentonite. Appl. Clay Sci. 65–66, 95–105.

Wang, Q., Cui, Y.J., Tang, A.M., Barnichon, J.D., Saba, S., Ye, W.M., 2013. Hydraulic conductivity and microstructure changes of compacted bentonite/san mixture during hydration. Eng. Geol. 164, 67–76.

Wang, G.F., Ran, L.Y., Xu, J., Wang, Y.Y., Ma, L., Zhu, R.L., Wei, J.M., He, H.P., Xi, Y.F., Xi, Y.F., Zhu, J.X., 2021a. Technical development of characterization methods provides insights into clay mineral-water interactions: a comprehensive review. Appl. Clay Sci. 206, 106088.

Wang, Y.P., Wang, Z., Zhao, Y., Yi, F.C., Zhu, B.L., 2021b. Swelling properties and permeability of GMZ bentonite-sand mixtures during different solutions infiltration. Sustainability 13, 1622.

Wen, Z.J., 2006. Physical property of China's buffer material for high level radioactive waste repositories. Chin. J. Rock Mech. Eng. 25, 794–800.

Xiong, Q., Jivkov, A.P., Ahmad, S.M., 2016. Modeling reactive diffusion in clays with two-phase-informed pore networks. Appl. Clay Sci. 119, 222–228.

Ye, W.M., Borrell, N.C., Zhu, J.Y., Chen, B., Chen, Y.G., 2014. Advances on the investigation of the hydraulic behavior of compacted GMZ bentonite. Eng. Geol. 169, 41–49.

Zhu, C.M., Ye, W.M., Chen, Y.G., Chen, B., Cui, Y.J., 2013. Influence of salt solutions on the swelling pressure and hydraulic conductivity of compacted GMZ01 bentonite. Eng. Geol. 166, 74–80.